Intermittent dust mass loss from activated asteroid P/2013 P5 (PANSTARRS)

F. Moreno

Instituto de Astrofísica de Andalucía, CSIC, Glorieta de la Astronomía s/n, 18008 Granada, Spain

fernando@iaa.es

J. Licandro

Instituto de Astrofísica de Canarias, c/Vía Láctea s/n, 38200 La Laguna, Tenerife, Spain,

and

Departamento de Astrofísica, Universidad de La Laguna (ULL), E-38205 La Laguna, Tenerife, Spain

C. Álvarez-Iglesias

Instituto de Astrofísica de Canarias, c/Vía Láctea s/n, 38200 La Laguna, Tenerife, Spain,

and

Departamento de Astrofísica, Universidad de La Laguna (ULL), E-38205 La Laguna, Tenerife, Spain,

and

GTC Project, E-38205 La Laguna, Tenerife, Spain

A. Cabrera-Lavers

Instituto de Astrofísica de Canarias, c/Vía Láctea s/n, 38200 La Laguna, Tenerife, Spain,

and

Departamento de Astrofísica, Universidad de La Laguna (ULL), E-38205 La Laguna, Tenerife, Spain,

and

GTC Project, E-38205 La Laguna, Tenerife, Spain

and

F. Pozuelos

Instituto de Astrofísica de Andalucía, CSIC, Glorieta de la Astronomía s/n, 18008 Granada, Spain

ABSTRACT

We present observations and models of the dust environment of activated asteroid P/2013 P5 (PANSTARRS). The object displayed a complex morphology during the observations, with the presence of multiple tails. We combined our own observations, all made with instrumentation attached to the 10.4m Gran Telescopio Canarias (GTC) on La Palma, with previously published Hubble Space Telescope (HST) images to build a model aimed at fitting all the observations. Altogether, the data cover a full 3-month period of observations which can be explained by an intermittent dust loss. The most plausible scenario is that of an asteroid rotating with the spinning axis oriented perpendicular to the orbit plane and loosing mass from the equatorial region, consistent with a rotational break-up. Assuming that the ejection velocity of the particles ($v \sim$0.02-0.05 m s^{-1}) corresponds to the escape velocity, the object diameter is constrained to $\sim$30-130 m for bulk densities 3000 to 1000 kg m^{-3}.

Subject headings: Minor planets, asteroids: individual (P/2013 P5 (PANSTARRS) — Methods: numerical

1. Introduction

Activated asteroid P/2013 P5 (PANSTARRS) was discovered by Pan-STARRS survey as a 21st magnitude comet on August 15.50, 2013 (Micheli et al. 2013). This object has a typical inner-belt asteroid orbit and yet displays a cometary-like tail, so it can be classified as a Main-belt comet (MBC). The object shares similar orbital elements with previously discovered disrupted asteroid P/2010 A2 (LINEAR) (Jewitt et al. 2010; Snodgrass et al. 2010; Moreno et al. 2013), both belonging to the Flora collisional family. The origin of activity taking place in the MBCs is unknown for most of the those objects. While some have been associated to impulsive events, such as collisions with another body or rotational break-up, other are most likely linked to water-ice sublimation. For reviews on those objects and the likely mechanisms involved in their activity, see e.g. Hsieh & Jewitt (2006), Bertini (2011), and Jewitt (2012).

A series of stunning images from the HST (Jewitt et al. 2013) at two epochs reveal the asteroid as a multiple-tailed object. Using the Finson-Probstein formalism, these tails have been associated to a series of ejection events at different dates, and the likely cause of the activity has been linked to a rotational disruption. In this paper, we present our own data, that were acquired during two months after the HST observations, and combine them with

the HST data. Our aim is then to monitor the activity scenario during a longer time frame and, mostly, to characterize the dust activity in terms of time variation of the mass loss, particle size distribution, and ejection velocities. Models mimicking an equatorial mass loss from the object have been incorporated in an attempt to investigate if a rotational disruption could be compatible with the ejection scenario.

2. Observations and data reduction

Images through Sloan r' and g' filters of P/2103 P5 were recorded under photometric and excellent seeing conditions (0.8-0.9″) on the nights of 2013 October 7 and 2013 November 8 (only r' images). We used the OSIRIS Optical System for Image and Low Resolution Integrated Spectroscopy (OSIRIS) camera-spectrograph (Cepa et al. 2000; Cepa 2010) at the GTC. The OSIRIS instrument consists of two Marconi CCD detectors, each with 2048×4096 pixels and a total unvignetted field of view of 7.8′×7.8′. The plate scale was 0.127 ″ px^{-1}, but we used a 2×2 pixel binning in order to improve the signal-to-noise ratio, so that the spatial resolution of the images becomes 222 km px^{-1} and 270 km px^{-1} at the observation dates. The images were bias and flat-field corrected using standard techniques, and calibrated in flux using standard stars. A sequence of five images per filter were obtained. An average image was then obtained from the available images by shifting and stacking the frames with respect to a reference frame by taking into account the object's sky motion. We estimate that as a result of both the flux calibration and the stacking procedure, the total flux uncertainty in the combined images is ∼0.1 mag. The final combined images are shown in Figure 1. The log of the observations is shown in Table 1. In that table, the apparent (m) and absolute (H) magnitudes of a region of 10 pixel aperture radius (2.5″ diameter) centered on the asteroid optocenter of each image is given. The absolute magnitude is given as $H = m - 2.5 \log(\Delta r_h) - \Phi(\alpha)$, where Δ and r_h are the geocentric and heliocentric distances of the asteroid, and $\Phi(\alpha)$ is the phase function, which is assumed to be that of an S-type asteroid, as most objects in the inner asteroid belt. The quantity $\Phi(\alpha)$ is computed by the Bowell et al. (1989) formalism, using a phase function parameter g=0.25, which is typical of S-type asteroids, the most common objects in the inner belt. The phase terms become $\Phi(17.7°)$=–0.81 on October 7, and $\Phi(27.0°)$=–1.07 on November 8, and the absolute magnitude $H_{r'}$ converges to the value $H_{r'}$=18.0±0.1 in both dates. To compare this value to the reported H_V by Jewitt et al. (2013) (H_V=18.69 on Sep. 10, and H_V=18.54 on Sep. 23), we need a transformation from r' to V magnitudes. Using the transformation equations of Fukugita et al. (1996), and the magnitude of the Sun in the standard Johnson-Cousins filter ($V_\odot$=–26.75, Cox 2000), we derive $r'_\odot$=–26.96. If the object follows a spectral dependence on wavelength similar to that of the Sun within the V and r' bandpasses (neutral color), the

V magnitudes can be obtained from the r' magnitudes by adding 0.21 magnitudes. Then, we would get H_V=18.2. This would indicate a brightness increase since Sep. 10 of ∼0.5 mag. This result immediately excludes a single event mechanism of dust ejection from the asteroid, as such event would have resulted in a brightness decrease as a function of time. Assuming that the brightness is entirely due to the asteroid, and not to the surrounding dust, this would led to an asteroid diameter of ∼590 m for a geometric albedo of p_v=0.29, typical of Flora family asteroids (Masiero et al. 2013). We will, however, assume that such brightness is entirely associated to the presence of dust surrounding the asteroid, and not to the presence of a nucleus, its contribution to the brightness being negligible. A justification of this hypothesis is given in the Results section on the basis of the low ejection velocities of the dust particles that we found in the modeling procedure.

3.   The Model

To perform the analysis of the images, we used our direct Monte Carlo dust tail model, as described in previous works (e.g., Moreno et al. 2012a; Fulle et al. 2010). In that model, we compute the trajectory of a large number of particles after being ejected from an asteroidal or cometary surface. Those particles move under the sole influence of the solar gravity and radiation pressure forces, describing a Keplerian orbit around the Sun. The orbital elements of each ejected particle are functions of the ejection velocity and the β parameter (e.g. Fulle 1989). This parameter can be written as $\beta = C_{pr}Q_{pr}/(2\rho r)$, where C_{pr}=1.19× 10^{-3} kg m^{-2}, Q_{pr} is the radiation pressure coefficient, and ρ is the particle density. The position of each particle in the plane of sky is then computed according to its orbital elements, and its contribution to the tail or coma brightness is evaluated, as a function of its size and geometric albedo. Owing to the many input models, we are forced to set some of them to a specific value. Then, the particles are considered spherical, their density is assumed at ρ_p=1000 kg m^{-3}, and their refractive index is set at $1.88 + 0.71i$, which is typical of carbonaceous composition (Edoh 1983). Using Mie theory, we find that the geometric albedo is $p_v \sim$ 0.04, and that the radiation pressure coefficient is $Q_{pr} \sim 1$ for particles of radius $r \gtrsim 1$ μm (Moreno et al. 2012a, their Figure 5). These choices of density and geometric albedo are highly arbitrary, since we do not know their real values, and were made actually to facilitate comparison with other MBCs analyzed, for which we assumed such values (e.g., Moreno et al. 2010, 2013).

We start by assuming an asteroid nucleus which is loosing mass from its equator, where centrifugal acceleration is maximum, uniformly in longitude. This would correspond to a mass loss scenario driven by a rotational disruption, as suggested by Jewitt et al. (2013).

This introduces three more model parameters to characterize the rotation properties: the orientation of the spinning axis with respect to the orbit plane, which is given by the obliquity, I, and the argument of the subsolar meridian at perihelion, Φ, and the rotational period, P (simple rotation is assumed). The nucleus is presumably very small, so that the rotation period should be very short, of the order of $P \lesssim 3$ h (Pravec et al. 2002). We assume $P=3$ h. The exact value of P does not influence the results if the tail age is much longer than that, as can be anticipated from the analysis by Jewitt et al. (2013). The rotation parameters I and Φ are set initially to $I=0°$, and $\Phi=0°$. To simplify, we also set all the possible time-variable parameters (except the dust mass loss rate) to a constant value. Thus, the size distribution power index is set to $\alpha=-3.5$, and the minimum and maximum particle sizes to 50 μm and 30 cm, respectively. These values were set after extensive experimentation with the code. Regarding velocities, we employed a function of the kind $v(\beta) = v_0\beta^\gamma$, were we adopt $\gamma=1/8$, i.e., a very weak dependence of $v(\beta)$ on β consistent with Moreno et al. (2012b) in their analysis of disrupted asteroid P/2012 F5 (Gibbs). The parameter v_0 and the dust mass loss rate as a function of the heliocentric distance are the fitting parameters.

4. Results

The times of significant dust ejection are first estimated from the best fitting synchrones to the dust tails. This procedure was applied to the HST images first, owing to their superb spatial resolution, and then to the GTC images. In the GTC images, the tails named A to F in Jewitt et al. (2013) (see Figure 2), the oldest being A, are sometimes blended because of poorer spatial resolution. Thus, in the GTC image of October 7, 2013, we have A, C/B, D, and E/F (see Figure 1). In addition, a younger tail not seen in the HST images (named G) appears. On the other hand, the last GTC image of November 8, 2013, does not show the complexity of the others, displaying a single and narrow tail extending to the northeast (see Figure 1). This is surely connected to the fact that the angle between Earth and the asteroid orbital plane (δ) is smaller than at the other dates (see Table 1).

The procedure was then to try different mass loss rates at those times, and set different ejection speeds (distinct v_0) until a good fit to the whole dataset (HST+GTC) is found in terms of dust tail brightnesses. The synthetic images corresponding to the GTC data are convolved with a point spread Gaussian function in order to take into account the seeing conditions during the observations. During the fitting procedure, we realized that to fit the length of tail "G" in the GTC 2013 October 7 image, we needed to set $r_{min}=10$ μm at the time of its peak emission, this being the only modification to the particle sizes in the time interval of ejection.

The results of the fits to the HST and GTC images are shown in Figures 2 (left panels) and 3. The model reproduces accurately all the features present in the HST and GTC images, in terms of brightness, length, and width. The dust loss rate profile corresponding to those fits is displayed in Figure 4, resulting in a total dust mass loss of 10^7 kg. The best fitted ejection velocity is given by $v = 0.12\beta^{1/8}$ m s^{-1}. This corresponds to ejection velocities ranging from about 0.02 m s^{-1} to 0.07 m s^{-1}, for 30 cm to 50 μm particles. We have also attempted to fit the images using a constant value for the ejection velocity for all the particles. We found very similar results to those of figures 2 (left panels) and 3 when a constant ejection velocity in the range 0.02 to 0.05 m s^{-1} is assumed. Regarding the maximum particle size ejected, we have verified that models having $r_{max} \gtrsim 1$ cm are compatible with the observations, provided the total mass ejected is modified accordingly. Thus, if r_{max} is set to its lowest acceptable limit, r_{max}=1 cm, the dust mass loss rate would be a factor of $\sim$5 smaller than that shown in figure 4, i.e., the total dust mass loss would become 2×10^6 kg. This constitutes the lower limit of ejected mass, for the assumed particle density of 1000 kg m^{-3}, and geometric albedo p_v=0.04.

The range of possible ejection velocities is 0.02-0.05 m s^{-1}. If these values are associated to escape velocities, this translates to possible asteroid diameters (assumed spherical) in the range 30 to 134 m, and masses in the range 4.6×10^7 to 1.3×10^9 kg, for assumed bulk densities of 1000 to 3000 kg m^{-3}. This size estimate is well below the upper limit of 480±80 m diameter derived by Jewitt et al. (2013) on the basis of magnitude measurements of the central condensation. As those authors recognize, this is an upper limit as the measurements could include near nucleus dust. We believe that it is indeed the case, in such a way that the magnitude of the central condensation is in fact attributable mainly to the dust around the nucleus, and not to the nucleus itself, whose contribution must be minimal according to the small size imposed by the escape velocity.

Concerning the rotational parameters of the asteroid, we started, as mentioned, from a scenario in which the rotating axis is perpendicular to the orbit plane (I=0°). We have generated synthetic images by varying both I, and Φ, in the full ranges, 0-180°, and 0-360°, respectively. We found that the only possible fits correspond to obliquities of either $I \sim 0°$ or, $I \sim 180°$, independently of Φ, i.e., with the rotating axis nearly perpendicular to the orbit plane, either pointing to the North or the South of the plane (prograde or retrograde motion). When the value of I departs significantly from either 0° or 180°, tails wider than observed are obtained.

Finally, we have also attempted to reproduce the observed brightness pattern using an isotropic ejection model, and the results we obtained for the GTC images are quite similar to those obtained with the above (anisotropic) model. However, the HST data are not well

reproduced with this isotropic ejection model, as the oldest tails, especially "B", "C", and "A" become significantly broader than observed. This is clearly shown in Figure 2, right panels.

5. Conclusions

From the Monte Carlo dust tail modeling of the observations of activated P/2013 P5 (PANSTARRS) we can extract the following conclusions:

1) The object has been subjected to an intermittent dust mass loss, most likely associated to a rotational disruption. This is confirmed from the analysis of both HST and GTC images. The total dust mass released was of the order of 10^7 kg, for particle density of 1000 kg m^{-3} and geometric albedo p_v=0.04.

2) The model of rotational disruption, based on simulations of an object that loose mass from its equatorial region, and whose rotational axis is perpendicular to its orbit plane, reproduces to the last detail the observed complex brightness pattern at four different epochs of HST and GTC observations. For obliquities different from 0° or 180°, the fits get much worse. On the other hand, an isotropic ejection model does not fit the HST data, because it produces much more diffuse tails than observed.

3) The ejection velocities are very low, of the order of 0.02-0.05 m s^{-1}. This places a limit to the size of the object as to be in the range 30-134 m for assumed densities of 3000 to 1000 kg m^{-3}.

REFERENCES

Bertini, I. 2011, Planet. Space Sci., 59, 365

Bowell,E., Hapke,B., Domingue,D., et al. 1989, in Asteroids II, University of Arizona Press, Tucson

Cepa, J., Aguiar, M., Escalera, V. et al. 2000, Poc. SPIE, 4008, 623

Cepa, J. 2010, Highlights of Spanish Astrophysics V, Astrophysics and Space Science Proceedings, Springer-Verlag, p. 15

Cox, A. 2000, Allen's Astrophysical Quantities (4th ed., New York: Springer)

Edoh, O. 1983, PhD thesis, Univ. Arizona

Fukugita, M., Ichikawa, T., Gunn, J. E., et al. 1996, AJ111, 1748

Fulle, M., 1989, A&A, 217, 283

Fulle, M., Colangeli, L., Agarwal, J., et al. 2010, A&A, 522, 63

Hsieh, H.H., & Jewitt, D. 2006, Science, 312, 561

Jewitt, D., Weaver, H., Agarwal, J. et al. 2010 Nature, 467, 817

Jewitt, D. 2012 AJ, 143, 21

Jewitt, D., Agarwal, J., Weaver, H., et al. 2013 ApJ, 778, L21

Masiero, J. R., Mainzer, A. K., Bauer, J. M., et al. 2013, ApJ, 770, 7

Micheli, M., Tholen, D. J., Primak, N., et al. 2013, Minor Planet Electronic Circulars, 37

Moreno, F., Licandro, J., G.-P. Tozzi, et al. 2010, ApJ, 718, L132

Moreno, F., Pozuelos, F., Aceituno, F., et al. 2012a, ApJ, 752, 136

Moreno, F., Licandro, J., & Cabrera-Lavers, A. 2012b, ApJ, 761, L12

Moreno, F., Licandro, J. & Ortiz, J.L 2013, ApJ, submitted

Pravec, P., Harris, A.W, & Michalowski, T. 2002, in Asteroids III, University of Arizona Press

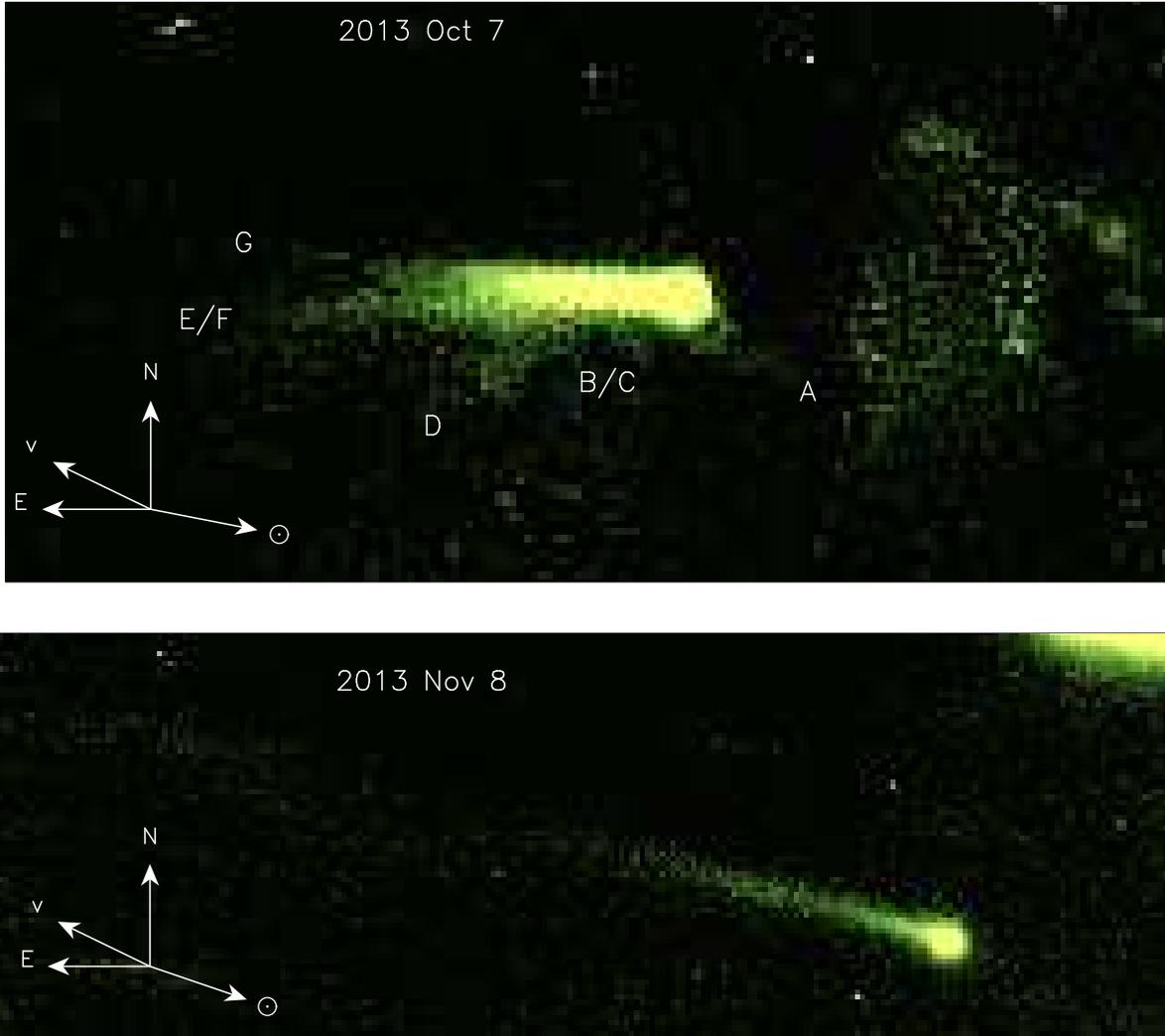Snodgrass, C., Tubiana, C., Vincent, J-B. et al. 2010 Nature, 467, 814

Fig. 1.— Stacked r' Sloan OSIRIS@GTC images of P/2013 P5 on the nights of UT 2013 October 7 (upper panel) and 2013 November 8 (lower panel). The dimensions of the upper and lower images are 35488×17744 km and 61939×21275 km, respectively. In the upper panel the different tails are marked. The nomenclature follows that of Jewitt et al. (2013). Tails marked as B/C and E/F are actually a blend of tails B and C, and E and F, respectively, as displayed in figure 1 of Jewitt et al. (2013). See also figure 2 in this paper. Note that tail G is the youngest tail, and does not appear in the HST observations. The directions of celestial North and East are indicated, as well as the direction to the Sun and the asteroid velocity vector.
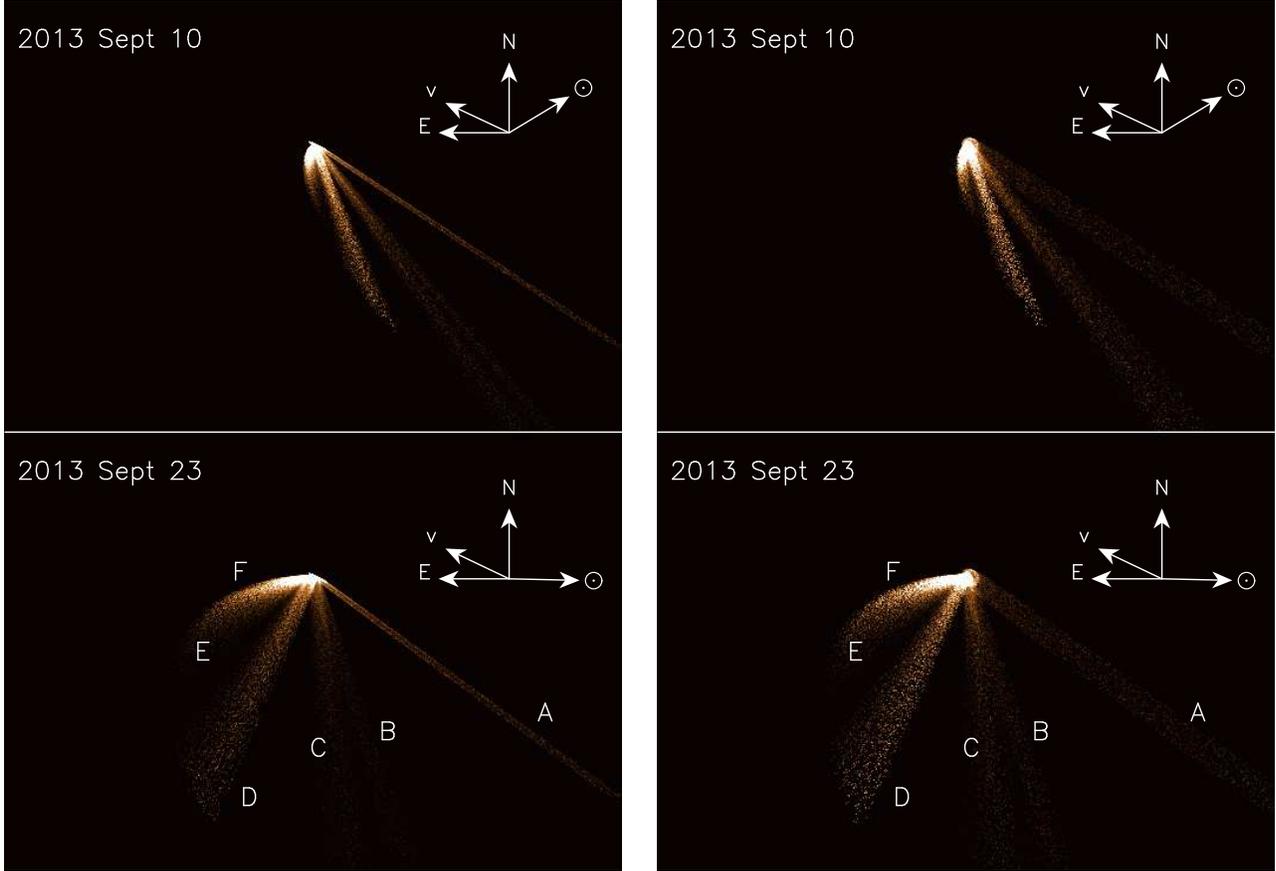
Fig. 2.— Model simulations of the Hubble Space Telescope images by Jewitt et al. (2013) (see their figure 1), at two epochs. The left panels correspond to an anisotropic ejection model, where the particles are ejected from the equator of a rotating nucleus with spin axis perpendicular to the orbit plane. The right panels correspond to an isotropic ejection model, with the same input parameters as the anisotropic model. In the lower panels, each tail is labeled according the nomenclature by Jewitt et al. (2013). The panels are 23000 km in width, the same as in figure 1 by Jewitt et al. (2013), to facilitate comparison. The directions of celestial North and East are indicated, as well as the direction to the Sun and the asteroid velocity vector.
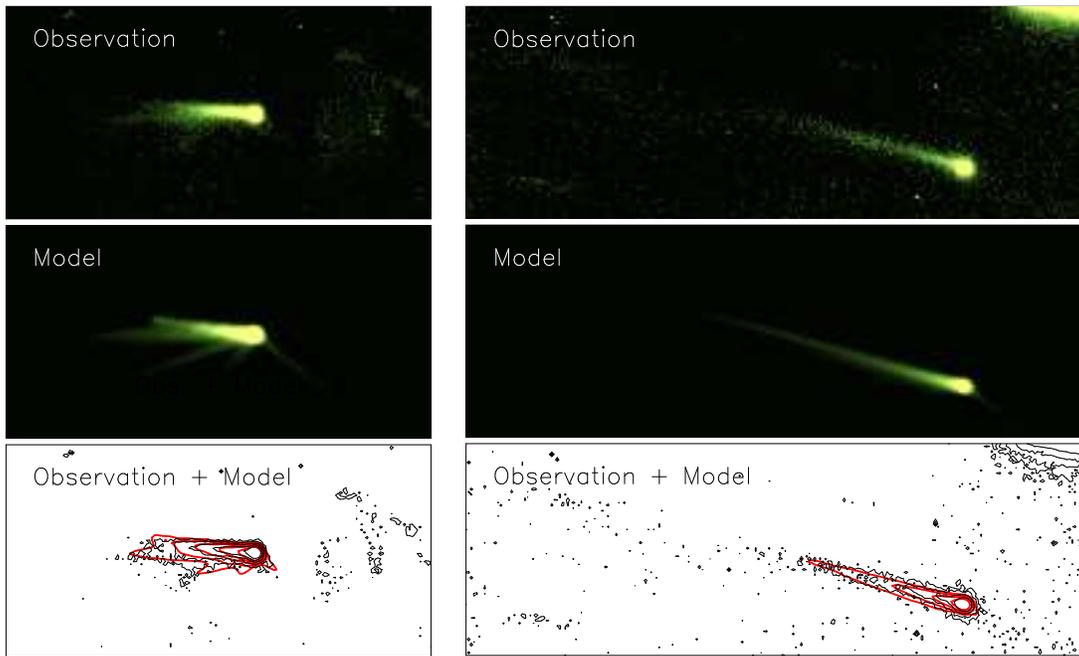
Fig. 3.— Left panels: observation and model simulation of the 2013 October 7 image. The lowermost panel show the comparison of the observed and modeled isophotes. The innermost isophote level is 3.8×10^{-14} solar disk intensity units, and the isophotes decrease in a factor of 2 between consecutive levels. Right panels: observation and model simulation of the 2013 November 8 image. The lowermost panel show the comparison of the observed and modeled isophotes. The innermost isophote level is 2×10^{-14} solar disk intensity units, and the isophotes decrease in a factor of 2 between adjacent levels. The dimensions of the images are the same as in Figure 1.
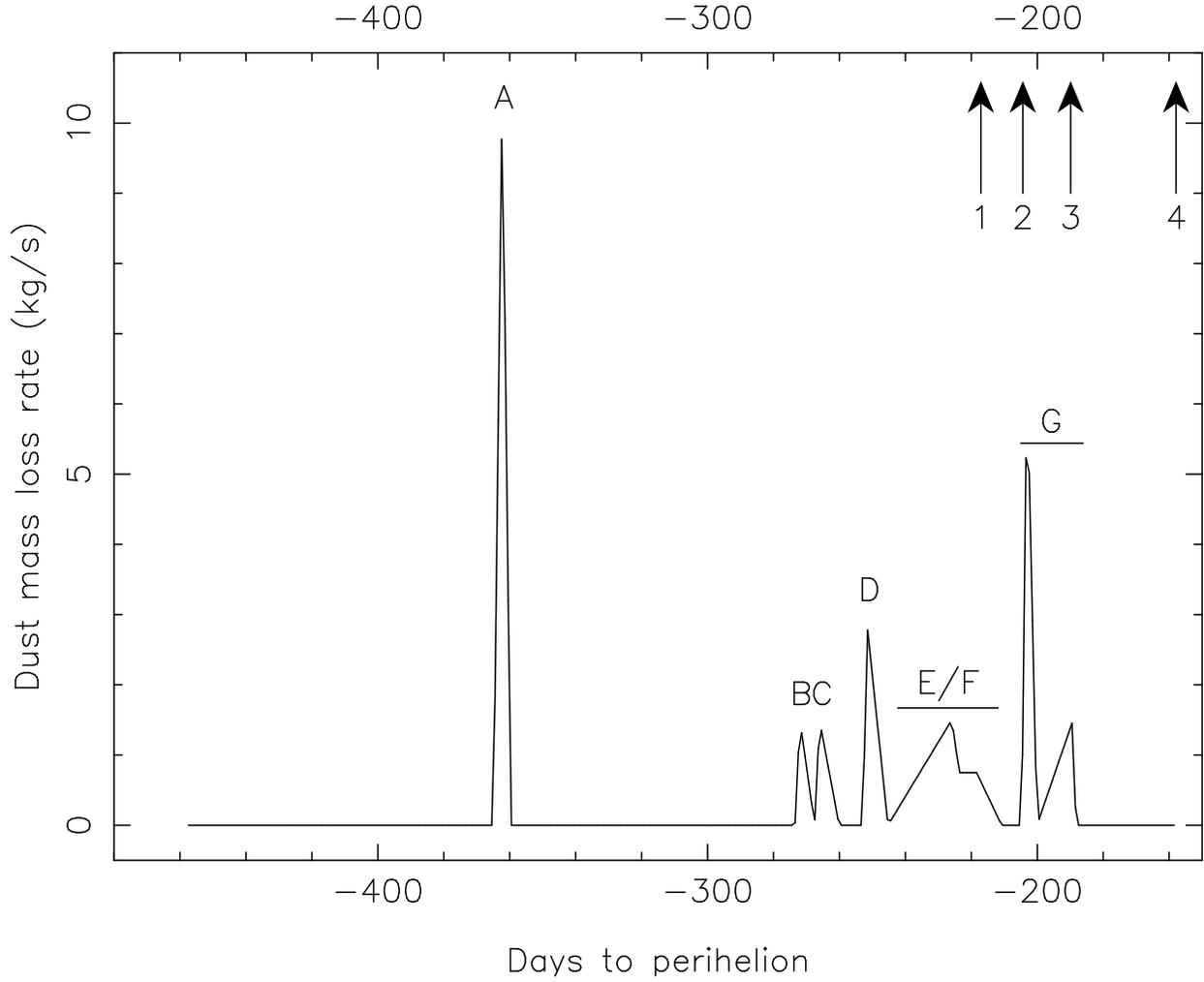
Fig. 4.— Modeled dust mass loss rate from P/2013 P5 as a function of time to perihelion. The sharp peaks of dust ejection are associated to the tails labeled "A" to "G" (see Figures 2 and 3). The arrows indicate the observation dates of the HST (1 and 2), and the GTC (3 and 4) data.

Table 1.   Log of the observations.

Date (UT)	r_h(AU)	Δ(AU)	$\alpha(°)$	$\delta(°)$	m	H
2013 Oct.7 22:18	2.077	1.204	17.7	−4.10	g'=21.3±0.1	18.5±0.1
2013 Oct.7 22:26	2.077	1.204	17.7	−4.10	r'=20.8±0.1	18.0±0.1
2013 Nov.8 21:04	2.038	1.462	27.0	−2.68	r'=21.5±0.1	18.0±0.1